

Multiobjective Optimization of CuO Nanolubricated Three-Lobe Journal Bearings Using Taguchi-GRA and TOPSIS Methods

Suman Kumar Mandal^{a,*} , Biplab Bhattacharjee^b , Nabarun Biswas^a , Kishan Choudhuri^a ,
Prasun Chakraborti^c 

^aDepartment of Production Engineering, NIT Agartala, Tripura, India,

^bDepartment of Mechanical Engineering, Faculty of Engineering and Technology, SRM Institute of Science and Technology, Ramapuram, Tamilnadu, India,

^cDepartment of Mechanical Engineering, NIT Agartala, Tripura, India.

Keywords:

Three-lobe bearings
CuO nanoparticles
Peak pressure
Frictional torque
GRA
TOPSIS

ABSTRACT

Three-lobe journal bearings are frequently used in high-speed rotating machinery due to their superior stability and load-carrying capacity over plain bearings. However, due to conflicting objectives like maximising peak pressure and minimising frictional torque, optimising their performance under nanolubricated conditions is still difficult. This study investigates the impact of copper-oxide (CuO) nanolubricants on the functionality of a three-lobe journal bearing is examined experimentally. Rotational speed (1000–2000 rpm), load (150–450 N), and nanoparticle concentration (0.05–0.10 wt.%) are all varied using a Taguchi L9 orthogonal array. For multiobjective optimisation, the Technique for Order Preference by Similarity to Ideal Solution (TOPSIS) and Grey Relational Analysis (GRA) were combined. The results of the analysis of variance showed that load is the main contributing factor (>94%). The optimal parameters determined by both GRA and TOPSIS are 1000 rpm, 450 N, 0.1% wt. concentration of CuO, which is then validated experimentally showing less than 5% error. Hence, the findings support a novel dual-optimization strategy for better bearing performance by confirming that CuO nanolubricants dramatically increase hydrodynamic pressure and decrease frictional torque.

* Corresponding author:

Suman Kumar Mandal 
E-mail: kumarsuman.nita@gmail.com

Received: 26 June 2025

Revised: 5 September 2025

Accepted: 18 October 2025



© 2025 Published by Faculty of Engineering

1. INTRODUCTION

The advancement of modern high-performance mechanical systems has increased demand for efficiency and reliability, especially in tribological

components. Journal bearings provide support for rotating shafts under radial loads, ensuring smooth rotation in high-speed operations and heavy load conditions, as seen in turbines, compressors, and engines [1]. Among the various

types of journal bearings, three-lobe journal bearings have garnered significant attention owing to their remarkable stability, superior dynamic performance, and enhanced load-bearing capacity compared with traditional circular or elliptical bearings [2]. Their asymmetric geometry redistributes hydrodynamic pressure, improving bearing stiffness and damping properties, while mitigating whirl instabilities at high speeds. This design creates complex pressure distribution in the lubricant film, requiring thorough analysis under various conditions [3]. While engine oils traditionally minimize friction between moving surfaces [4], they often prove inadequate for modern machinery operating under increased thermal stress and higher velocities. The integration of nanoparticles into base lubricants has significantly improved tribological performance [5,6]. The complex interaction of rotational speed, load, and nanoparticle concentration necessitates statistical and computational techniques for effective system optimization [7-9]. The following discussion reviews the literature concerning various computational and optimization strategies, as well as the application of nanolubricants in journal bearings.

Marey [10] investigated pressure distribution in fluid film bearings using SAE5W30, SAE10W40, and SAE20W50 oils at speeds from 50 to 400 rpm under constant load. SAE 5W30 oil showed lower efficiency, performing best up to 150 RPM, with decreased effectiveness at 400 RPM. The study found a correlation between the oil film pressure distribution and both the rotational speed and oil viscosity. Singh [11] studied pressure distribution in twin-groove journal bearings using SAE15W40, SAE20W40, and refined oil. The results showed that the pressure increased with the load, and the pressure profile of the twin-grooved bearings resembled that of the single-grooved bearings. Bouyer and Fillon [12] analyzed the torque generated during journal bearing start-up by adjusting the pressure. Four bearings were tested to evaluate the friction coefficient under various feeding conditions, lengths, and clearances. Their findings showed that the torque increased during start-up at a specific pressure. Maurya et al. [13] found frictional torque rises with shaft speed until stabilizing at top speed. Shinde and Pawar [14] used gray relational analysis to optimize journal

bearing parameters, minimizing friction while maximizing load capacity. Avikal et al. [15] varied the load, speed, and attitude angle to improve the oil film thickness using Grey-based Taguchi optimization, highlighting the impact of the angle on the bearing performance. Sun et al. [16] established criteria for optimizing crankshaft bearing designs to lower shaft mass from friction loss. Biswas et al. [17] used MOGA to optimize oil film thickness and pressure in three-lobe journal bearings. Shinde et al. [18] showed that modifying groove region, width, depth, pitch and grooves improved fluid film bearings performance. Mandal et al. [19] reviewed nanofluid applications in hydrodynamic journal bearings, noting improvements through nanoparticle lubrication. Biswas et al. [20] reviewed effects of nanoparticle-based lubricants on journal bearing performance, covering nanoparticle selection, dispersion mechanisms, and improvements. Biswas et al. [21] used DoE-RSM strategy to optimize tribological behaviors for energy efficiency. Mandal et al. [22] demonstrated Taguchi-based optimization for improving journal bearing performance. Baskar and Sriram [23] investigated bearing material wear using pin-on-disk testing with nanoparticle-based rapeseed oil, chemically treated rapeseed oil and SAE20W40. The results showed that CuO decreased the friction coefficient by 18% compared to SAE20W40 and 49% for modified rapeseed oil. Srinivas et al. [24] tested SAE90 and SAE20W40 oils to examine pressure distribution, finding SAE90 handled greater loads than SAE20W50. Jamalabadi [5] investigated nanolubricants in journal bearings using SAE20W50 base fluid and Reynolds equation. The results showed that the nanoparticles enhanced the mass coefficient, damping ratio, and stiffness. Lanes and Flack [25] investigated the effects of preload, load angle, and offset factor on threshold instability in three-lobe bearings and found a decreased load angle dependency with an increased offset. Biswas et al. [26] studied three-lobe journal bearing performance, showing increased load led to higher pressure profiles and temperatures. Flack and Allaire [27] evaluated nine three-lobe bearings by varying preload and load angle, finding consistency between theoretical and experimental relationships at low preloads. Li et al. [28] compared multilobe journal bearings, with elliptical bearings showing superior stability at high and medium loads. Aher et al. [29] and Biswas et al. [30] demonstrated

three-lobe journal bearings' superior load capacity versus plain bearings. Rahmatabadi et al. [31] found increased load capacity with micropolar lubrication in three-lobe bearings. Sharma et al. [32] studied wear defects in two-lobe hybrid bearings, showing decreased fluid film thickness with 50% wear defect. Research [33-36] has confirmed the superior stability of lobed bearings in high-speed rotating equipment. Kumar and Kakoty [37] studied three-lobe bearings using TiO₂ nanolubricant, finding increased load capacity and flow coefficient, reduced friction, and improved stiffness. Shooroki et al. [38] studied two-lobe bearings with SiO₂-multiwall carbon nanotubes/SAE40 hybrid nanofluid. Higher nanoparticle volume enhanced pressure distribution, load capacity, and viscosity while reducing attitude angle and temperature. Tala-Ighil et al. [39] showed micro-texturing improved load capacity and stability in hydrodynamic journal bearings. Kumar and Kakoty [40] analyzed three-lobe bearings with TiO₂-based lubricant, showing improved flow coefficient, load capacity, and stability. Solghar [41] studied oil with Al₂O₃ nanoparticles, examining side leakage, load capacity, friction coefficient, and temperature-pressure distribution. The nanoparticles increased the load capacity by 17.7% while reducing the flow rate. Nicoletti [42] investigated the heat capacity of lubricants using ISO VG 68 oil with Si, SiO₂, Al, Al₂O₃, Cu, and CuO nanoparticles. Higher volumetric heat capacity improved load capacity by 10%, with CuO showing best results. Kalakada et al. [43] studied journal bearings with CuO, CeO₂, and Al₂O₃ nanoparticle lubricants, finding minimal effects under isoviscous conditions but significant improvements under thermoviscous conditions.

The studies [2,17,25-36] concluded that multilobe bearings are better than plain journal bearings. While numerous studies have investigated nanoparticles in plain journal bearings [44-50], research on lobe bearings with nanoparticles remains limited. Most studies use numerical and analytical methods to predict the performance characteristics. Experimental investigations on multilobe bearings with nanoparticle additives are particularly limited. Copper oxide (CuO) has emerged as a highly effective additive owing to its antiwear properties, thermal conductivity, and friction-reducing capabilities. The present work provides

an experimental investigation of three-lobe journal bearings under nanolubrication using CuO nanoparticles, where a Taguchi L9 orthogonal array assesses the influence of three input parameters—rotational speed, load, and CuO nanoparticle weight concentration—on two output responses: peak pressure and frictional torque. The peak pressure indicates the load-handling capacity, whereas the frictional torque is related to energy loss and thermal loading. Optimal lubrication aims to maximize the peak pressure while minimizing the frictional torque; however, these objectives conflict, requiring multi-objective optimization techniques. This study uses two multi-criteria decision-making (MCDM) techniques: Grey Relational Analysis (GRA) and the Technique for Order Preference by Similarity to Ideal Solution (TOPSIS). The GRA transforms a multi-response optimization problem into a single gray relational grade, simplifying the identification of optimal settings [14]. This is advantageous when the input-output relationships are complex or experimental data are limited [51]. TOPSIS ranks alternatives based on the geometric proximity to an ideal solution, considering the best and worst values of each criterion, providing a perspective on the performance of parameter combinations [52]. Comparative studies in tribology and manufacturing [15,53] have shown that these methods yield consistent yet complementary outcomes. Their combined application in the experimental optimization of nanolubricated three-lobe bearings remains unreported, forming a unique contribution to this study.

2. GEOMETRY OF THREE-LOBE JOURNAL BEARING

As illustrated in Figure 1, the bearing comprises three lobes, each equidistantly positioned from the bearing's midpoint, a characteristic referred to as ellipticity. These lobes extend to a maximum arc of 120° but are interspersed with axial grooves that facilitate oil entry. This lobe configuration enhances the stability and load-bearing capacity of the bearing, particularly under high-speed conditions [14]. The load-carrying capability of the bearing is attributed to the hydrodynamic pressure generated within the lubricant film between the rotating shaft and lobed surfaces. In addition to permitting oil entry into the clearance area, grooves improve stability compared to plain bearings.

Table 1. Literature review summary.

Study	Bearing Type	Nanoparticle	Methodology	Key Findings	Gap Addressed by Present Study
Kumar & Kakoty (2020) [37]	Three-lobe	TiO ₂	Analytical	Enhanced load capacity, reduced friction	No experimental validation
Rasoolizadeh et al. (2022) [38]	Two-lobe	Hybrid nanofluid	Analytical	Improved stability and film thickness	Lacked experimental evidence
Yasir et al. (2023) [47]	Plain	TiO ₂ , ZnO	Experimental	Better thermal performance and reduced wear	Not applied to three-lobe bearings
Biswas et al. (2024) [20]	Plain	Base oil grades	RSM Based Optimization method	Improved energy efficiency	No nanolubricant involvement
Present study	Three-lobe	CuO	Experimental + GRA-TOPSIS	Optimized peak pressure & frictional torque	First experimental study with CuO nanoparticle-based lubricants + dual MCDM in three-lobe bearings

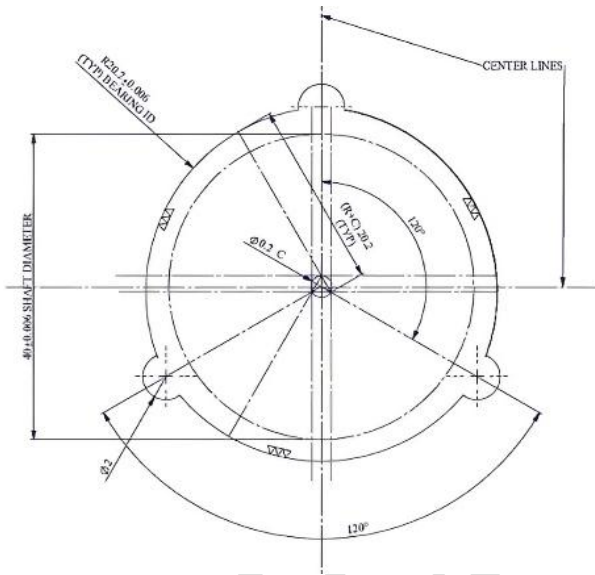


Fig. 1. Three-lobe bearing layout. [30].

The Reynolds equation can be employed to analyze three-lobe bearings because it elucidates the hydrodynamic lubrication process in journal bearings. For incompressible and steady-state flow conditions, the two-dimensional version of the Reynolds equation is applicable, which is

$$\frac{\partial}{\partial x} \left(h^3 \frac{\partial p}{\partial x} \right) + \frac{\partial}{\partial z} \left(h^3 \frac{\partial p}{\partial z} \right) = 6\eta U \frac{\partial h}{\partial x} \quad (1)$$

Where:

p = hydrodynamic pressure,

h = lubricant film thickness,

η = dynamic viscosity of the lubricant,

U = surface speed of the journal,

x and z = coordinates in the axial and circumferential directions, respectively.

In a three-lobe bearing, lobe configuration determines film thickness h , expressed as a function of eccentricity ϵ and angular position θ . This thickness is:

$$h(\theta) = c(1 + \epsilon \cos(\theta - \theta_0)) \quad (2)$$

Where:

c = radial clearance of the bearing,

ϵ = eccentricity ratio,

θ_0 = angular position of the minimum film thickness.

3. MATERIALS AND METHODS

3.1 Experimental configuration

The Journal Bearing Test Rig (JBTR), shown in Figure 3, evaluates the bearing performance under various conditions by measuring the frictional torque, oil film pressure, and speed. A variable-speed motor drives a shaft connected to brass three-lobe bearings via a metal bellows linkage and a torque load cell. The bearing housing includes a stepper motor-driven indexing mechanism for 90° rotations up to 180° for the pressure measurements. The pressure sensor recorded the oil film pressure, along with the torque and speed data. The deadweight mechanism applies a radial load, with bearings submerged in the lubricant. Data from the sensors were transmitted to a computer for analysis. The pressure sensor accuracy is $\pm 0.25\%$ of full scale and torque cell resolution is ± 0.5 Nmm. The JBTR includes data acquisition, controllers, lubrication systems, loading mechanisms and software interfaces.

Figure 2 shows the three-lobe bearing assembly, and Figure 3 shows the complete configuration, with the specifications listed in Table 2.

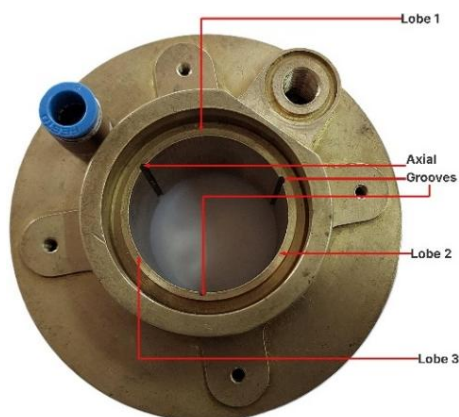


Fig. 2. Three-lobe bearing.

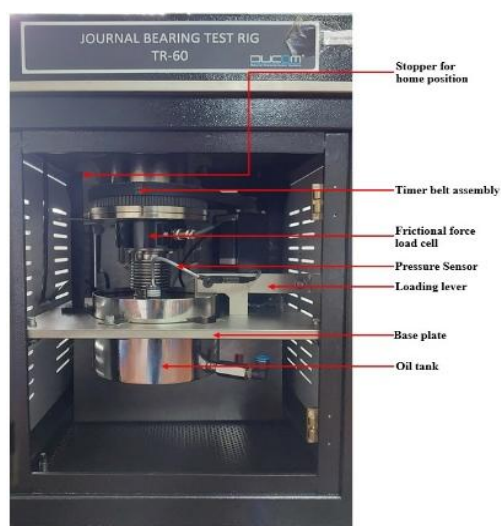


Fig. 3. Journal bearing test rig.

Table 2. Mechanical and test specification.

Specifications	Brass Bearing System
Test bearing size	Material: Brass 60-40%, pressure tested for leakage inner \varnothing 40mm.
Journal Outer Diameter & Material	EN-8 bearing steel, hardened to 60 Hrc, ground to 0.6 Ra surface roughness, \varnothing 40mm.
Journal Speed	150-2000 rpm
Loading ratio	1:5
Self-weight of loading lever	35N
Oil Tank Capacity	2.8 litres
Pulley ratio (Speed)	1:1
Radial Load	150-750 N
c/r ratio	0.005
Length/ dia (l/d) ratio	1:1
Radial clearance	0.1 mm

3.2 Characterization of copper oxide (CuO) nanoparticles

Research-grade CuO nanoparticles (30-50 nm) were obtained from Ultrananotech Private Limited, India. X-Ray Diffraction (XRD) analysis was used to investigate their crystalline structure. Figure 4 shows the XRD pattern with sharp diffraction peaks, indicating highly crystalline nanoparticles. Peaks observed at 111, -111, 111, -202, 020, 202, -113, 022, 220, 311, -222 matched the standard diffraction data for monoclinic CuO, confirming phase purity within the 2θ range of 20° to 90° . Scanning Electron Microscopy (SEM) was used to evaluate the morphology. Figure 5 shows nearly spherical morphology with slight agglomeration owing to van der Waals forces. The particle size distribution matched the supplier specifications.

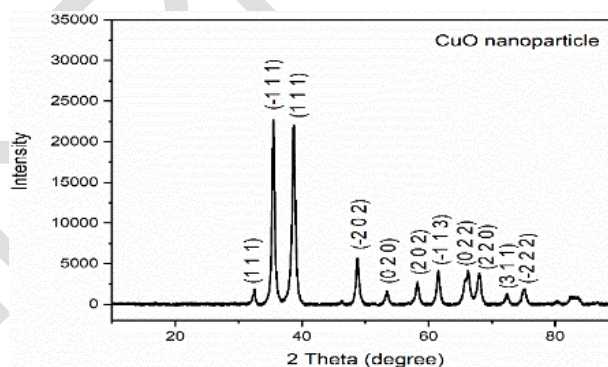


Fig. 4. XRD pattern of CuO nanoparticles.

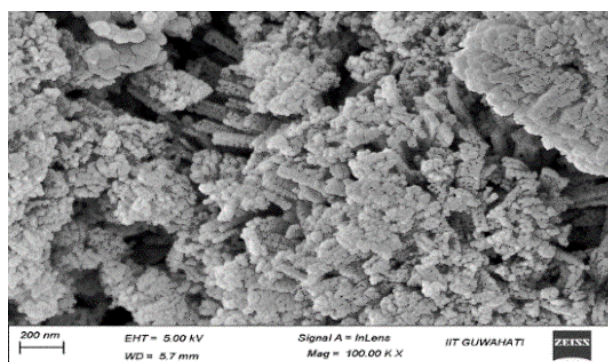


Fig. 5. SEM image of CuO nanoparticles.

3.3 Nanolubricant preparation

The synthesis of nanolubricants involves incorporating nanoparticles into a base oil, where a stable and homogeneous dispersion is crucial for maintaining tribological properties. Various methods exist for nanofluid preparation, with an emphasis on preventing particle agglomeration. Researchers have used

surfactants, surface modification techniques, and mechanical dispersion methods, such as ultrasonication, to obtain stable suspensions. Nanolubricant preparation techniques are categorized into single- and two-step physical methods [54]. Chemical methods offer alternative synthesis routes that may enhance dispersion stability [55-60]. This study used a two-step method for nanolubricant preparation (Figure 6) because of its cost-effectiveness and suitability for large-scale production [61-63]. Copper Oxide (CuO) nanoparticles were synthesized separately and integrated into the base lubricant. SAE10W40 engine oil is used as the base fluid. Three samples were formulated with CuO nanoparticles at weight concentrations of 0.05%, 0.075%, and 0.1%. Oleic acid was used as a surfactant at 1% of the oil weight to reduce agglomeration and enhance stability. The nanoparticles were gradually introduced into the base oil while stirring with a magnetic stirrer for 24 h. The suspension then underwent probe ultrasonication for 60 min to break nanoparticle clusters and achieve uniform distribution. The prepared nanolubricants were stored in airtight containers and stirred before each experimental run to ensure homogeneity. Figure 7 shows the prepared copper-oxide-based nanolubricant samples. Stability was studied using the sedimentation method. The nanolubricants were stored for 15 days, showing no significant settling for 2 days; however, sediments formed at the bottom after 15 days.



Fig. 6. Two-step method preparation of nanolubricant.

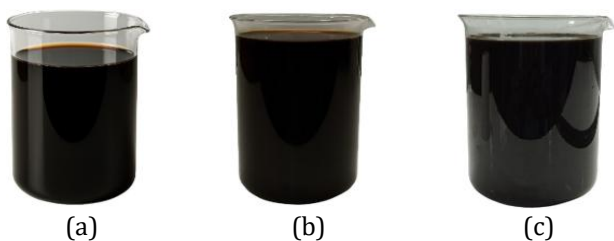


Fig. 7. Prepared Samples with wt. concentration of (a) 0.05% (b) 0.075% (c) 0.1%.

3.4 Design of experiments

Design of Experiments (DOE) is a statistical methodology for systematic experiment planning, analysis of input factors, and process optimization while minimizing resources. DOE identifies individual and interactive effects of variables on outcomes. The Taguchi method, among DOE techniques, is favored for its efficiency in multi-parameter optimization with fewer trials. Using an L9 orthogonal array, this study investigated three primary input parameters on three-lobe journal bearing performance with CuO-based nanolubricants. The Taguchi L9 orthogonal array is selected because it allows for the efficient examination of three factors at three levels using only nine trials, as opposed to the L16, L27 Taguchi design. This reduction is particularly important in nanolubricant experiments, where both preparation and testing require significant resources. Previous studies have confirmed the dependability of the L9 array in tribological and machining research, including the optimization of journal bearings [14,15], machining of titanium alloys with EDM and lathe [64,65], and nanofluid-assisted machining [66]. Therefore, the L9 design offers a practical compromise between the statistical reliability and experimental cost-effectiveness. The operating parameters are selected based on an analysis of the journal bearing test rig conditions, equipment limits, and literature. The rotational speed ranges from to 1000-2000 RPM in 500 RPM increments. The Radial loads of 150, 300, and 450 N represented light to moderate loads, chosen based on the test rig capacity and the nanoparticle concentrations of 0.05%, 0.075%, and 0.1% are selected from the literature [5,8,14,48], providing effective dispersion and enhanced performance without aggregation. These parameters ensured a meaningful investigation of the peak pressure and frictional torque while maintaining experimental feasibility. The factors and levels are listed in Table 3.

Table 3. Factors and levels in experiment.

Factors	Level 1	Level 2	Level 3
Speed (RPM)	1000	1500	2000
Load (N)	150	300	450
CuO Concentration (% wt.)	0.05	0.075	0.1

The L9 orthogonal array design evaluates three parameters using nine trials compared to 27 trials in a complete factorial design. This reduction makes the Taguchi method advantageous when resources are limited while maintaining reliable system insights. For each trial, two output responses were measured.

- Peak pressure (indicator of load-carrying capacity)
- Frictional torque (indicator of energy loss and thermal loading)

The experimental results are presented in Table 3.

3.5 GRA

In contexts where the simultaneous optimization of multiple output parameters is required, Grey Relational Analysis (GRA) offers an effective and practical methodology [14]. As a multi-criteria decision-making (MCDM) technique, GRA transforms diverse performance characteristics into a singular grey relational grade (GRG), thereby facilitating the identification of optimal process conditions [67].

This research utilized GRA to enhance the two primary performance metrics of the journal bearing system: maximizing peak pressure and minimizing frictional torque. The following steps were used to conduct the GRA:

Step 1: Data Normalization

The experimental data for each response were first normalized to ensure comparability, using different normalization techniques depending on the desired objective:

For larger-the-better responses (peak pressure), the normalization formula used is:

$$X_i^*(k) = \frac{X_i(k) - \min X(k)}{\max X(k) - \min X(k)} \quad (3)$$

For smaller-the-better responses (frictional torque), the normalization formula used is:

$$X_i^*(k) = \frac{\max X(k) - X_i(k)}{\max X(k) - \min X(k)} \quad (4)$$

Where:

$X_i^*(k)$ = normalized value

$X_i(k)$ = experimental data value

Step 2: Grey Relational Coefficient (GRC)

Once normalized, the Grey Relational Coefficient (GRC) for each response was calculated to express the relationship between the ideal (best) and actual normalized data:

$$\xi_i(k) = \frac{\Delta_{min} + \zeta \Delta_{max}}{\Delta_i(k) + \zeta \Delta_{max}} \quad (5)$$

Where:

$$\Delta_i(k) = |X_0^*(k) - X_i^*(k)|$$

$\Delta_{min}, \Delta_{max}$ = minimum and maximum of $\Delta_i(k)$.

ζ is the distinguishing coefficient, generally taken as 0.5 to provide equal weighting.

Step 3: Grey Relational Grade (GRG)

The Grey Relational Grade (GRG) was then determined by averaging the GRC values for the two responses for each experiment:

$$\gamma_i = \frac{1}{n} \sum_{k=1}^n \xi_i(k) \quad (6)$$

Where:

γ_i is the GRG for the i-th experiment.

The experimental trial with the highest GRG value is considered the optimal combination of input parameters [64].

3.6 Technique for Order Preference by Similarity to Ideal Solution (TOPSIS)

MCDM, a branch of operations research, enables evaluation and ranking of alternatives based on performance criteria set by decision-makers, particularly for conflicting criteria. Given the dynamic nature of multi-criteria decisions, decision-makers must analyze potential consequences [52,53,68]. The TOPSIS method [69], among MCDM techniques, is popular due to its computational simplicity, mathematical foundation, and user-friendliness. The initial step in the TOPSIS methodology involves creating a decision or evaluation matrix, which illustrates how the alternatives under consideration perform across different criteria.

$$Z = \begin{bmatrix} z_{11} & z_{12} & \dots & z_{1n} \\ z_{21} & z_{22} & \dots & z_{2n} \\ \dots & \dots & \dots & \dots \\ z_{m1} & z_{m2} & \dots & z_{mn} \end{bmatrix} \quad (7)$$

where z_{ij} denotes the performance metric of the i^{th} option in relation to the j^{th} criterion, whilst m represents the total number of options and n signifies the quantity of criteria or attributes. The criteria can be categorized into two types: beneficial, where higher values are advantageous, and non-beneficial, where lower values are preferred. This approach establishes two benchmarks: positive and negative ideal solutions. The positive ideal solution aims to maximize the beneficial criteria while minimizing the non-beneficial criteria, whereas the negative ideal solution does the opposite. In the context of the given MCDM problem, the optimal alternative is identified as the one closest to the positive ideal solution and furthest from the negative ideal solution. The Euclidean distances of all alternatives from both ideal solutions were calculated, and the alternatives were ranked according to these distances. The TOPSIS method comprises the following steps [70]:

Step 1: Normalization of decision matrix

Given that the components of the initial decision matrix comprise data with varying scales and dimensions, it is imperative to initially normalise them into a dimensionless matrix to facilitate equitable comparison of the criteria under consideration:

$$e_{ij} = \frac{z_{ij}}{\sqrt{\sum_{i=1}^m z_{ij}^2}} \quad (8)$$

Where e_{ij} is the normalized value of z_{ij} .

Step 2: Weighted normalized matrix computation (v)

$$v_{ij} = w_j * e_{ij} \quad (9)$$

Where w_j is the weight of j^{th} criterion.

Step 3: Evaluation Ideal and Negative-Ideal Solutions

Ideal Solution (Best Case):

$$A^+ = \{max(v_{ij}) \mid j \in J, min(v_{ij}) \mid j \in J'\} \quad (10)$$

where J represents positive criteria and J' represents negative criteria.

Negative-Ideal Solution (Worst Case):

$$A^- = \{min(v_{ij}) \mid j \in J, max(v_{ij}) \mid j \in J'\} \quad (11)$$

Step 4: Separation measures calculation (S)

To measure separation measures we use the Euclidean distance of v_{ij} from v_j^+ and v_j^- .

$$S_i^+ = \sqrt{\sum_{j=1}^n (v_{ij} - v_j^+)^2} \quad (12)$$

$$S_i^- = \sqrt{\sum_{j=1}^n (v_{ij} - v_j^-)^2} \quad (13)$$

Where S_i^+ represents the separation between the i^{th} option and the best case, whilst S_i^- denotes the gap between the i^{th} option and the worst case.

Step 5: Determination of relative proximity to the optimal solution (C_i).

$$C_i = \frac{S_i^-}{S_i^+ + S_i^-} \quad (14)$$

Step 6: Experiments ranking

In this step we rank the experimental solutions in descending order of C_i value. The highest value is selected as the optimal solution indicating that it is nearest to positive ideal case and away from negative ideal case.

3.7 Anova

The relationship between a dependent variable and one or more independent variables can be examined and demonstrated using Analysis of Variance (ANOVA). In the context of the JBTR process, ANOVA's main objective is to identify which parameters significantly impact quality attributes. The importance of modifying the JBTR process parameters for these features is determined by analyzing how much the sum of squares contributes to the total variation. To identify process parameters that significantly impact quality characteristics, the Fisher-developed F-test is utilised. From a statistical standpoint, the F-test helps ascertain whether the observed differences are genuine. When F values are higher, it suggests that certain procedural parameters result in notable performance improvements. For factors with a high percentage contribution, minor adjustments can lead to substantial performance effects [21].

3.8 Experimental procedure

The journal is attached to a spindle with brass bearings and is fixed to the base plate of the

Journal Bearing Test Rig (JBTR). A pulley system driven by an AC motor enabled the journal rotation. The bearings maintained uniform length-to-diameter ratios to minimize side leakage. The bearing body has oil supply holes for lubricant flow into the pressure sensor mounting areas. An indexing pulley with a load cell connected to a stepper motor that rotated up to 180° in 90° increments, aligning the bearing housing with the load direction. The radial loading mechanism includes a linkage device connecting a loading pallet for weights (150-600 N) and a ball bearing that transfers the load to the journal. Brass bearings receive lubrication from a dual unit, with the lubricant drawn from a lower base plate oil pan and delivered through a gravity feed. An upper-plate collection pan manages the circulation. The controller unit displays the film pressure, angular position, and frictional torque data, which are transmitted to a computer for analysis. The software generates real-time plots, or the data can be recorded manually. Each test requires a 20-minute cooling period to ensure thermal stabilization and consistent operating conditions, as temperature changes affected the pressure and torque readings.

3.9 Methodology

A methodology combining experimental research with multi-criteria decision-making (MCDM) techniques is used to evaluate a three-lobe journal bearing under nanolubricated conditions. Copper oxide (CuO) nanoparticles were dispersed in SAE10W40 oil at concentrations of 0.05%, 0.075%, and 0.1%. Using a Taguchi L9 orthogonal array, the rotational speed, radial load, and nanoparticle concentration were varied. The peak pressure and frictional torque were measured using a journal bearing test rig with computerized data acquisition. The data were analyzed using Grey Relational Analysis (GRA) and the Technique for Order Preference by Similarity to Ideal Solution (TOPSIS) to determine the optimal parameters. Analysis of Variance (ANOVA) was used to assess the significance of each input factor, and interaction plots as well as contour plots is used to visualize the effects of the parameters on the bearing performance. The methodology for Taguchi-GRA method and Taguchi-TOPSIS method are shown in Figure 8 and Figure 9.

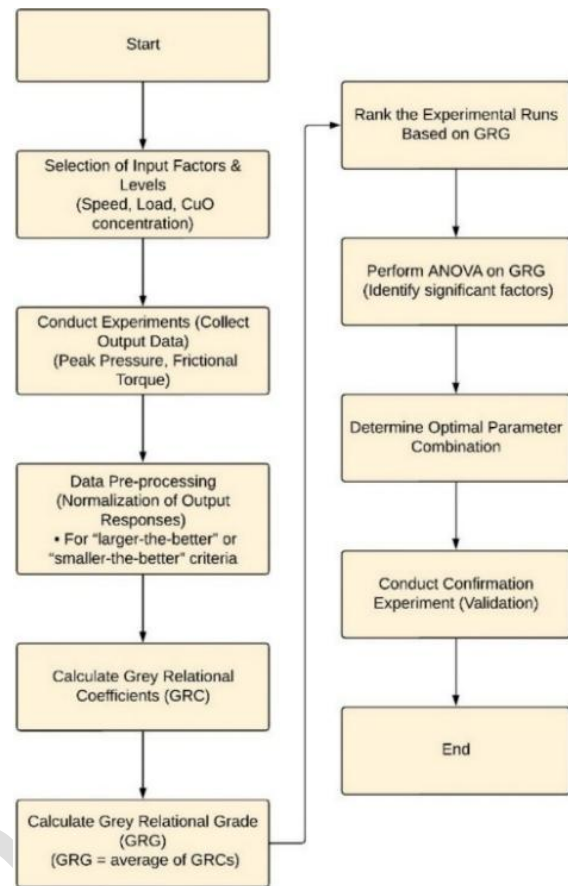


Fig. 8. Flowchart for Taguchi-GRA method.

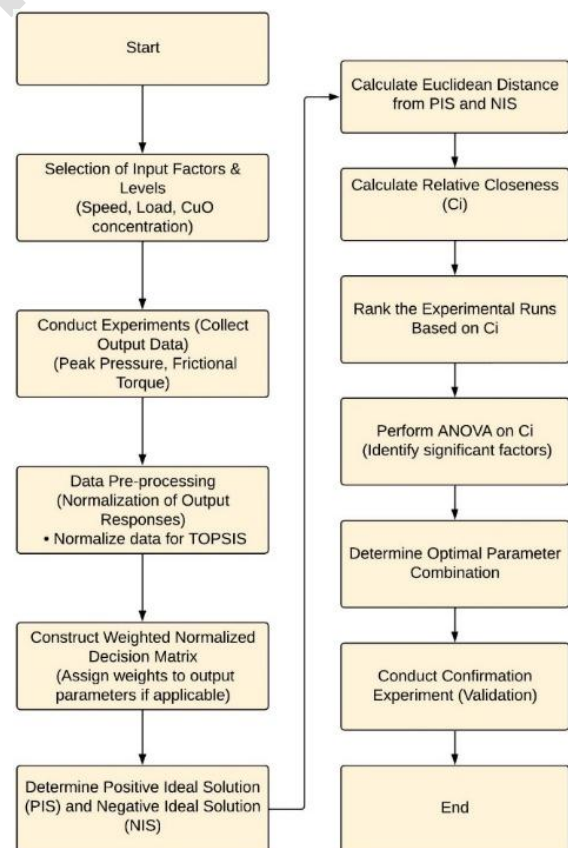


Fig. 9. Flowchart for Taguchi-TOPSIS method.

4. RESULTS AND DISCUSSIONS

This study examines how rotational speed, applied load, and CuO nanoparticle concentration affect peak pressure and frictional torque in a three-lobe journal bearing. Total of nine experimental trials were conducted using Taguchi's L9 orthogonal array design, with each trial repeated twice for reliability. In the current study, all designs, plots, and analyses were conducted using the statistical software Minitab

18. The experimental results are shown in Table 4. The measured peak pressure ranged from a minimum of 50 psi (Trial 1) to a maximum of 396 psi (Trial 3). The frictional torque ranged from a minimum of 185 Nmm to a maximum of 397 Nmm for the nine Taguchi experiments. The model's highest peak pressure and lowest frictional torque occurred at a combination of 1000 rpm, a load of 450 N, and a 0.1 wt.% CuO concentration, which showed substantial hydrodynamic performance.

Table 4. Experimental data.

Exp. No.	Speed (rpm)	Load (N)	Wt. Concentration (%)	Peak Pressure (psi)	Frictional Torque (Nmm)
1	1000	150	0.050	50	354
2	1000	300	0.075	226	263
3	1000	450	0.100	396	185
4	1500	150	0.075	54	397
5	1500	300	0.100	220	281
6	1500	450	0.050	371	300
7	2000	150	0.100	60	340
8	2000	300	0.050	198	378
9	2000	450	0.075	370	300

4.1 Model evaluation

The ANOVA of the peak pressure and frictional torque (Tables 5 and 6) shows that all process parameters have statistically significant effects on the bearing performance (95% confidence level) with p-values below 0.05. For peak pressure, load is most dominant at 99.41%, CuO concentration at 0.34%, and speed at 0.20%. The regression model showed good accuracy with a small standard error ($S=3.59320$), $R^2=99.96\%$, adjusted $R^2=99.93\%$, and predicted $R^2=99.86\%$, suggesting negligible variation. For frictional torque, the load had the greatest effect (46.04%), followed by CuO concentration (25.11%) and speed (22.94%). The model showed good fit statistics ($S=20.0111$, $R^2=94.09\%$, adjusted $R^2=90.55\%$, predicted $R^2=81.47\%$). The contour plots (Figures 11 and

12) for peak pressure and frictional torque showed the combined influence of speed (rpm), load (N), and CuO weight concentration (%) on the responses. The analysis indicated that load was the primary parameter that increased both responses, whereas speed and concentration effects were minimal. As the concentration and load increased, the effects became more pronounced, with pressure increasing and frictional torque decreasing at low speeds, demonstrating the favorable tribological effects of CuO nanoparticles. The presented results describe the relative impact of every input factor on the total variation of responses in the entire experiment and not an optimum situation only. For instance, the load range as the consistently dominant factor affecting the variation in both peak pressure and frictional torque throughout the range of operation.

Table 5. ANOVA analysis for peak pressure.

Source	DF	Seq SS	Contribution	Adj SS	Adj MS	F-Value	P-Value
Speed (rpm)	1	323	0.20%	323	323	24.99	0.004
Load (N)	1	157788	99.41%	157788	157788	12221.11	0.000
Wt. Concentration (%)	1	542	0.34%	542	542	41.94	0.001
Error	5	65	0.04%	65	13		
Total	8	158717	100.00%				

Table 6. ANOVA analysis for frictional torque.

Source	DF	Seq SS	Contribution	Adj SS	Adj MS	F-Value	P-Value
Speed (rpm)	1	7776	22.94%	7776	7776.0	19.42	0.007
Load (N)	1	15606	46.04%	15606	15606.0	38.97	0.002
Wt. Concentration (%)	1	8513	25.11%	8513	8512.7	21.26	0.006
Error	5	2002	5.91%	2002	400.4		
Total	8	33897	100.00%				

Residual examination of both response variables (Figures 10 and 11) indicated that the models were adequate. Normal probability plots showed linear trends and confirmed the residual normality. Histograms displayed symmetrical distributions, while residuals versus fits and observation order plots showed no patterns, indicating homoscedasticity and the absence of autocorrelation. These results validate the models that predict the bearing performance under nanolubricated conditions.

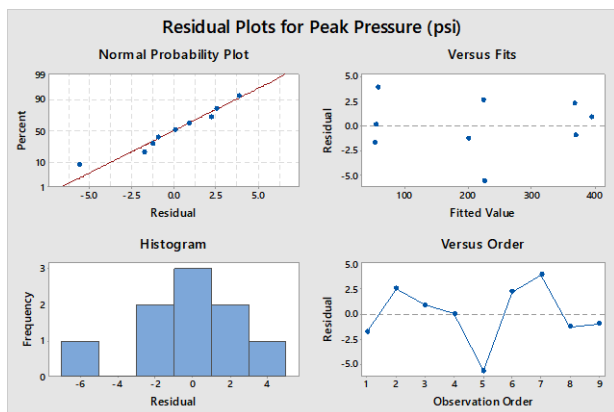


Fig. 10. Peak Pressure's Residual Plots.

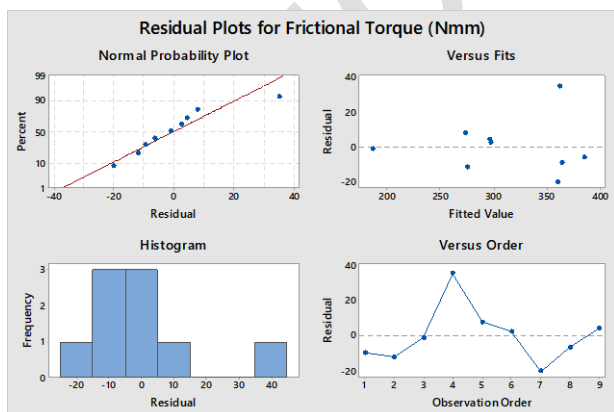


Fig. 11. Residual Plots for Frictional Torque.

The contour plots (Figures 12 and 13) for peak pressure and frictional torque showed the combined influence of speed (rpm), load (N), and CuO weight concentration (%) on the responses. The analysis indicated that load was

the primary parameter that increased both responses, whereas speed and concentration effects were minimal. As the concentration and load increased, the effects became more pronounced, with pressure increasing and frictional torque decreasing at low speeds, demonstrating the favorable tribological effects of CuO nanoparticles.

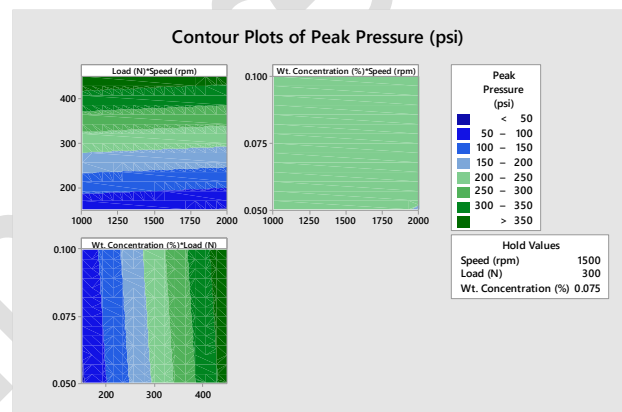


Fig. 12. Contour plots illustrate the influence of (a) Load and Speed, (b) Wt. concentration and Speed, and (c) Wt. concentration and Load on peak pressure (psi).

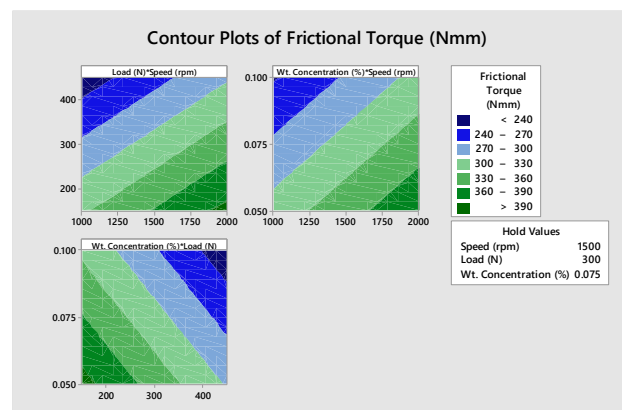


Fig. 13. Contour plots illustrate the influence of (a) Load and Speed, (b) Wt. concentration and Speed, and (c) Wt. concentration and Load on frictional torque (Nmm).

The Interaction plots (Figures 14 and 15) show a strong linear relationship between the load and peak pressure and a significant load-

concentration interaction on the frictional torque as the concentration increased with the load under high-load conditions, reducing the frictional torque with an increasing number of nanoparticles.

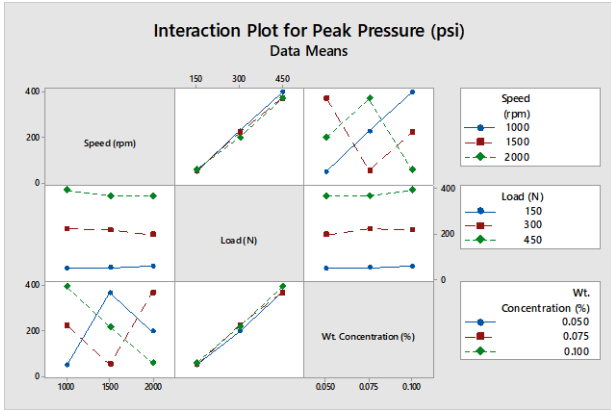


Fig. 14. Interaction plots for peak pressure depict the interplay among Speed, Load, and CuO nanoparticle concentration.

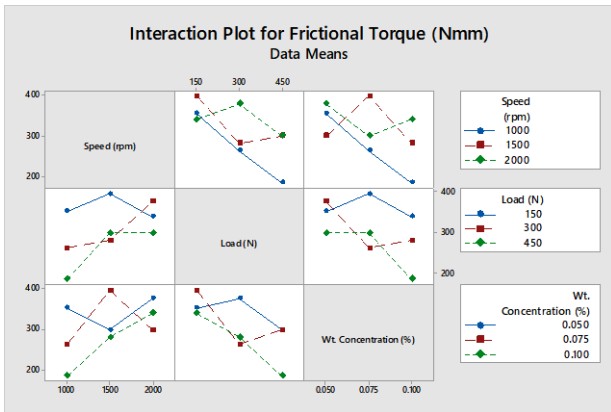


Fig. 15. Interaction plots for frictional torque depict the interplay among Speed, Load, and CuO nanoparticle concentration.

The mathematical equation that describes the relationship between pressure, frictional torque and the specified input parameters are as follows:

$$\begin{aligned}
 \text{i. Peak Pressure (psi)} &= -114.72 \\
 &- 0.01467 \text{ Speed (rpm)} \\
 &+ 1.08111 \text{ Load (N)} \\
 &+ 380.0 \text{ Wt. Concentration (\%)}
 \end{aligned} \quad (15)$$

$$\begin{aligned}
 \text{ii. Frictional Torque (Nmm)} &= 417.9 + 0.0720 \text{ Speed (rpm)} \\
 &- 0.3400 \text{ Load (N)} \\
 &- 1507 \text{ Wt. Concentration (\%)}
 \end{aligned} \quad (16)$$

4.2 Viscosity measurement

The viscosity of CuO-based nanolubricant were measured using Brookfield Digital. The prepared samples were poured in a 100 ml beaker for viscosity measurements. During pre-testing the dynamic viscosity of 0.05%, 0.075% and 0.1% wt. concentration of nanoparticles based lubricant are 167.7, 173.8 and 175.2 centipoise (cP) at 100 rpm. Post testing the same viscosities were 42.8, 45.5 and 48.4 centipoise (cP) at 100 rpm. A sample image for viscosity measurement procedure for 0.1% wt. concentration of CuO based nanolubricant pre-testing has been shown in Figure 16.



Fig. 16. Viscosity measurement for 0.1% wt. concentration of CuO based nanolubricant pre-testing.

4.3 Multiobjective Optimization using GRA

Grey Relational Analysis (GRA) determines optimal combinations of input parameters—rotational speed, applied load, and CuO nanoparticle weight concentration—by evaluating their influence on maximizing peak pressure while minimizing frictional torque. GRA optimizes multiple responses with varying units and scales. The experimental data is normalized using "larger-the-better" criterion for peak pressure and "smaller-the-better" criterion for frictional torque (Equations 3 and 4) to achieve comparable dimensionless ranges. Grey Relational Coefficients (GRCs) are calculated using Equation 5, with a distinguishing coefficient ($\zeta = 0.5$) balancing maximum and minimum deviation effects. The Grey Relational Grade (GRG) is determined using Equation 6 by averaging the GRCs, assuming equal importance of objectives. Trials with highest GRG values represent optimal balance between pressure generation and frictional resistance reduction.

Table 7. Optimization using GRA.

Sl. No.	Output Parameters		Grey relational coefficients (ξ_i)		Grey relational grade (γ_i)	Rank
	Peak Pressure (psi)	Frictional Torque (Nmm)	Peak Pressure (psi)	Frictional Torque (Nmm)		
1	50	354	0.333333333	0.385454545	0.359393939	8
2	226	263	0.504373178	0.576086957	0.540230067	4
3	396	185	1	1	1	1
4	54	397	0.33592233	0.333333333	0.334627832	9
5	220	281	0.495702006	0.524752475	0.51022724	5
6	371	300	0.873737374	0.479638009	0.676687691	2
7	60	340	0.339882122	0.406130268	0.373006195	7
8	198	378	0.466307278	0.35451505	0.410411164	6
9	370	300	0.869346734	0.479638009	0.674492371	3

Table 8. Analysis of variance for grey relational grade (γ_i).

Source	DF	Seq SS	Contribution	Adj SS	Adj MS	F-Value	P-Value
Speed (rpm)	1	0.03252	8.82%	0.03252	0.032519	5.50	0.066
Load (N)	1	0.27484	74.54%	0.27484	0.274841	46.51	0.001
Wt. Concentration (%)	1	0.03179	8.62%	0.03179	0.031790	5.38	0.068
Error	5	0.02954	8.01%	0.02954	0.005909		
Total	8	0.36869	100.00%				

Among the trials (Table 7), Trial 3 attained the highest γ_i value of 1, indicating the most effective equilibrium between the elevated peak pressure and diminished frictional torque. This trial corresponds to the optimal parameter combination in the experimental setup. According to the ANOVA results (Table 8), the applied load significantly influenced the Grey Relational Grade, accounting for 74.54% of the total variation ($P = 0.001$), highlighting its primary role in overall performance. In contrast, the rotational speed and nanoparticle weight concentration contributed 8.82% and 8.62%, respectively, and exhibited nearly significant effects ($P \approx 0.066$ and 0.068 , respectively), suggesting a moderate impact. The model's

residual error was 8.01%, indicating a strong fit and reliable optimization results using the GRA method.

4.4 Multiobjective optimization using TOPSIS

The TOPSIS Method is used to identify the optimal solution from experimental data by determining ideal input parameters—rotational speed, applied load, and nanoparticle weight concentration—that enhance peak pressure while minimizing frictional torque. This method enables varying importance levels for each objective function, evaluating trade-offs between maximizing peak pressure and minimizing frictional torque.

Table 9. Optimization using TOPSIS.

Sl. No.	Output Parameters		S_i^+	S_i^-	C_i	Rank
	Peak Pressure (psi)	Frictional Torque (Nmm)				
1	50	354	0.244103839	0.022615747	0.084792225	8
2	226	263	0.118996766	0.135427341	0.532289736	4
3	396	185	0	0.253216438	1	1
4	54	397	0.250859358	0.002628275	0.010368455	9
5	220	281	0.126185966	0.127277176	0.502152601	5
6	371	300	0.062674942	0.217001351	0.775901842	2
7	60	340	0.235345425	0.030690637	0.115362695	7
8	198	378	0.165014433	0.097758274	0.37202598	6
9	370	300	0.062850355	0.216362754	0.774901849	3

Table 10. Analysis of Variance for C_i .

Source	DF	Seq SS	Contribution	Adj SS	Adj MS	F-Value	P-Value
Speed (rpm)	1	0.020979	2.17%	0.020979	0.020979	12.40	0.017
Load (N)	1	0.912819	94.40%	0.912819	0.912819	539.39	0.000
Wt. Concentration (%)	1	0.024678	2.55%	0.024678	0.024678	14.58	0.012
Error	5	0.008462	0.88%	0.008462	0.001692		
Total	8	0.966938	100.00%				

Weights of 0.5 (as used in [14]) are allocated to both peak pressure and frictional torque, prioritizing peak pressure maximization while addressing frictional torque reduction. To ensure comparability between objectives with different units, normalization is applied using Equation 8, followed by conversion to weighted normalized values using Equation 9. The ideal solution performance measures are [0.260199, 0.097300], while negative ideal solutions are [0.032853, 0.2088012]. Separation measures are calculated using Equations 12 and 13, from which closeness coefficient values are derived using Equation 14. Results with the highest closeness coefficients are selected.

As illustrated in Table 9, Trial 3 attained the highest closeness coefficient ($C_i = 1$), indicating the most advantageous equilibrium between elevated pressure and reduced friction. Trials 6 and 9 follow closely with $C_i \approx 0.775$, corroborating their nearly optimal performance. The ANOVA results presented in Table 10 reveal that the applied load significantly influenced the TOPSIS closeness coefficient (C_i), accounting for 94.40% of the total variation ($P = 0.000$), thereby

establishing it as the most impactful input factor. Both rotational speed and nanoparticle concentration exerted smaller yet statistically significant effects ($P = 0.017$ and $P = 0.012$, respectively), contributing 2.17% and 2.55% to the performance variability, respectively. With an error contribution of only 0.88%, this highlights the reliability and robustness of the TOPSIS-based optimization method in identifying ideal operating parameters.

4.5 Validation and discussions

A linear regression model (Equations 15 and 16) validates the selection of independent variables within the model range. Confirmatory experiments were conducted using the trial 3 setup (1000 RPM rotational speed, 450 N applied load, 0.1 wt.% CuO nanoparticle concentration) evaluated optimal parameters from Taguchi-GRA and Taguchi-TOPSIS methods. This setup maximized the peak pressure while minimizing the frictional torque. The results were compared with the predicted outcomes from multi-objective optimization models, as shown in Table 11.

Table 11. Confirmation experiment results.

Speed (rpm)	Load (N)	Wt. Concentration (%)	Peak Pressure (psi)			Frictional Torque (Nmm)		
			Theo. (Eq. 15)	Exp.	Error (%)	Theo. (Eq. 16)	Exp.	Error (%)
1000	450	0.1	395.11	378	4.33	186.20	194	4.19

Table 11 shows the minimal error margins, underscoring the precision of the models in determining the optimal conditions for nanolubricated three-lobe journal bearings. This validation highlights the efficacy of integrating Taguchi-based Design of Experiments (DOE) with Multi-Criteria Decision-Making (MCDM) methods, such as Grey Relational Analysis (GRA) and the Technique for Order of Preference by Similarity to Ideal Solution (TOPSIS), for complex tribological optimization challenges.

This study aimed to enhance a three-lobe journal bearing system using copper oxide (CuO)-based nanolubricants through experimental methods and multicriteria decision-making. The objective was to optimize the system by maximizing the pressure and minimizing the frictional torque using the Taguchi design, Grey Relational Analysis (GRA), and TOPSIS. The ANOVA results showed that the applied load was the most significant factor, accounting for 99% of the peak pressure

variation and 94% of the TOPSIS closeness coefficient. This aligns with the hydrodynamic bearing characteristics, where an increased load creates a higher film pressure through the shaft-bushing interaction [17, 37]. The interaction plots showed that speed and nanoparticle concentration had minor effects, except at higher loads. The influence of the CuO nanoparticle concentration increased at higher loads, reducing the frictional torque through improved film stability and thermal conductivity [23, 42]. GRA and TOPSIS identified Trial 3 (speed: 1000 RPM, Load: 450 N, % Wt. Concentration: 0.1) as the optimal operating parameters. The alignment of the Grey Relational Grades and TOPSIS coefficients validated these MCDM techniques with the Taguchi DOE. While previous studies [14, 15] used single-objective methods, integrating dual optimization methods enhanced the robustness of the results. Validation experiments showed minimal error (<5%) between the predicted and observed values, confirming the system reliability and CuO nanoparticle suitability for industrial applications.

In addition to validating the optimization framework, it is essential to evaluate the practical feasibility and implications of CuO-based nanolubricants in three-lobe journal bearings. This involves considering the economic aspects, performance enhancement through hybrid nanofluids, and limitations of the nanoparticle concentration.

(i) Cost-Benefit Analysis: Nanolubricant preparation requires investment in nanoparticle procurement and dispersion. However, this cost is offset by the operational benefits. The study showed reduced frictional torque (up to 40–50%) and increased peak pressure using 0.1 wt.% CuO nanolubricant compared with base oil. These improvements reduce power losses and surface wear, extending the bearing life and reducing maintenance. In high-speed equipment, these advantages lead to reduced downtime and lower life-cycle costs. Previous analyses [42,54,70] indicate short payback periods when maintenance and energy savings were considered. Therefore, despite the higher initial costs, the overall cost-benefit balance favors critical applications that require high operational reliability.

(ii) Potential for Hybrid Nanofluids: While single-component nanolubricants show significant tribological improvements, studies [38,54] suggest that hybrid nanofluids—combining two or more nanoparticles—can offer synergistic effects. Hybrid nanofluids provide enhanced thermal conductivity, dispersion stability, and antiwear properties for bearings under severe conditions. Multiple nanoparticles promote rolling action and surface passivation, stabilizing lubrication. For three-lobe journal bearings, hybrid formulations improve load capacity and reduce friction. Future studies may apply the optimization framework (Taguchi-GRA-TOPSIS) to hybrid nanofluids to identify ideal concentration ratios and parameters.

(iii) Limitations - Viscosity Increase at Higher Concentrations: Increasing the CuO concentration from 0.05 wt. % to 0.1 wt.% raises dynamic viscosity, potentially increasing shear forces and pumping power requirements. Beyond a critical concentration, the load enhancement benefits may be offset by increased viscous drag and potential thermal instability. Kalakada et al. [43] and Kwak & Kim [60] highlighted the trade-off between concentration and hydrodynamic efficiency. The optimal concentration must balance the enhanced tribological behavior with a manageable viscosity.

(iv) Relevance to Automotive and Aerospace Applications: The findings have direct implications for high-performance bearings in the automotive and aerospace sectors. Enhanced peak pressure and reduced frictional torque using CuO nanolubricants improve the load-carrying capacity and energy efficiency, which are crucial for fuel efficiency and component longevity. The dual-optimization methodology offers a systematic approach to parameter selection in these industries.

5. CONCLUSIONS AND FUTURE SCOPES

This study analyzed the optimization of a three-lobe journal bearing using copper oxide (CuO) nanolubricants under varying rotational speeds, applied loads, and nanoparticle concentrations. The aim was to balance peak pressure maximization and frictional torque minimization through experimental optimization. The following conclusions can be drawn:

(i) The GRA and TOPSIS optimization results were consistent, identifying 1000 RPM speed, 450 N load, and 0.1 wt.% CuO concentration as optimal settings for highest peak pressure and lowest frictional torque. This convergence across the two MCDM methods validates the effectiveness of dual-method optimization for tribological systems.

(ii) The experimental results provide insights into the tribological performance of journal bearings using nanolubricants. The applied load was the dominant factor, accounting for 94% of the GRA and TOPSIS variations, which is consistent with the hydrodynamic lubrication principles. Rotational speed remained significant at higher nanoparticle concentrations, while CuO concentration showed moderate effects under high loads by reducing metal contact and improving thermal conductivity.

(iii) The experimental validation reinforced the accuracy of the proposed models. The results of the confirmatory experiments closely matched the predictions from the GRA and TOPSIS analyses. The percentage error between the predicted and observed results for the peak pressure and frictional torque remained below 5%, within the acceptable tribological testing uncertainty. This validation demonstrates the practical applicability of the optimization framework in bearing systems across different geometries and lubricants.

(iv) CuO nanoparticles as lubricant additives showed advantages over traditional lubrication by enhancing the load-carrying capacity and reducing friction under high loads. The nanoparticles acted as micro-rolling elements, reducing the surface roughness and improving the thermal dissipation, thereby creating a stable lubrication regime. These benefits align with previous studies showing the effectiveness of metal oxide nanoparticles in reducing friction and wear in journal bearings.

(v) Unlike prior research on plain bearings and theoretical modeling, this study experimentally examined a three-lobe bearing under nanolubricated conditions. The dual-optimization approach provides a comprehensive view of performance trade-offs, making the findings applicable to engineering designers who balance multiple objectives under constraints.

The future scopes for the present study are investigating diverse nanoparticles (e.g. Al_2O_3 , TiO_2 , or hybrid nanofluids (CuO-TiO_2)) in a variety of lubrication situations; using CFD/FEM verification to study both pressure distribution and film thickness; and finally assessing long-term durability to assess the realistic usability of the systems.

REFERENCES

- [1] S. Gao, H. Ding, K. Cheng, S. Chen, and H. Fu, "Computational design and analysis of aerostatic journal bearings with application to ultra-high-speed spindles," *Proc. Inst. Mech. Eng. Part C: J. Mech. Eng. Sci.*, vol. 231, no. 7, pp. 1205–1220, 2016, doi: [10.1177/0954406216639344](https://doi.org/10.1177/0954406216639344).
- [2] O. Pinkus, "Analysis and Characteristics of the Three-Lobe Bearing," *J. Basic Eng.*, vol. 81, no. 1, pp. 49–55, 1959, doi: [10.1115/1.4008359](https://doi.org/10.1115/1.4008359).
- [3] A. Chasalevris, "Analytical Evaluation of the Static and Dynamic Characteristics of Three-Lobe Journal Bearings with Finite Length," *J. Tribol.*, vol. 137, no. 4, 2015, doi: [10.1115/1.4030023](https://doi.org/10.1115/1.4030023).
- [4] J. Sun, Y. Fu, M. Deng, and C. Gui, "Thermohydrodynamic Lubrication Analysis of Misaligned Plain Journal Bearing with Rough Surface," *J. Tribol.*, vol. 132, no. 1, 2010, doi: [10.1115/1.4000515](https://doi.org/10.1115/1.4000515).
- [5] M. Y. Abdollahzadeh Jamalabadi, L. K. B. Li, S. Leveneur, M. Safdari Shadloo, W.-M. Yan, and R. Alamian, "Effects of Nanoparticle Enhanced Lubricant Films in Thermal Design of Plain Journal Bearings at High Reynolds Numbers," *Symmetry*, vol. 11, no. 11, p. 1353, 2019, doi: [10.3390/sym11111353](https://doi.org/10.3390/sym11111353).
- [6] Y. J. Jason, H. G. How, Y. H. Teoh, and H. G. Chuah, "A Study on the Tribological Performance of Nanolubricants," *Processes*, vol. 8, no. 11, p. 1372, 2020, doi: [10.3390/pr8111372](https://doi.org/10.3390/pr8111372).
- [7] K. G. Ravindra and T. Nagaraju, "Optimization of hydrodynamic journal bearing: MOGA approach," *AIP Conf. Proc.*, vol. 2390, no. 1, p. 020012, 2022, doi: [10.1063/5.0076823](https://doi.org/10.1063/5.0076823).
- [8] S. B. Kalakada, R. K. P. K, and P. N. N. Kumarapillai, "Static characteristics of thermohydrodynamic journal bearing operating under lubricants containing nanoparticles," *Ind. Lubr. Tribol.*, vol. 67, no. 1, pp. 38–46, 2015, doi: [10.1108/ilt-01-2013-0015](https://doi.org/10.1108/ilt-01-2013-0015).
- [9] H. Hirani, "Multiobjective optimization of a journal bearing using the Pareto optimality concept," *Proc. IMechE, Part J: J. of Eng. Tribol.*,

- vol. 218, no. 4, pp. 323–336, 2004, doi: [10.1243/1350650041762668](https://doi.org/10.1243/1350650041762668).
- [10] N. Marey, "An Experimental Investigation of Hydrodynamic Journal Bearing with Different Oil Grades," Port Said Eng. Res. J., vol. 23, no. 2, pp. 46–54, 2019, doi: [10.21608/pserj.2019.49576](https://doi.org/10.21608/pserj.2019.49576).
- [11] M. Singh, "Experimental Investigation of twin Groove Hydrodynamic Journal bearing with different Hydraulic Oils (15W40, 20W40, Refined Oil)," Int. J. Adv. Res. Innov., vol. 3, no. 2, pp. 136–140, 2015, doi: [10.51976/ijari.321529](https://doi.org/10.51976/ijari.321529).
- [12] J. Bouyer and M. Fillon, "Experimental measurement of the friction torque on hydrodynamic plain journal bearings during start-up," Tribol. Int., vol. 44, no. 7–8, pp. 772–781, 2011, doi: [10.1016/j.triboint.2011.01.008](https://doi.org/10.1016/j.triboint.2011.01.008).
- [13] A. Maurya, A. Kumar, and A. D. Punia, "CFD and Frictional Torque Analysis of Hydrodynamic Journal Bearing," Int. J. Eng. Res. Technol., vol. 8, no. 7, pp. 959–968, 2019.
- [14] A. B. Shinde and P. M. Pawar, "Multi-objective optimization of surface textured journal bearing by Taguchi based Grey relational analysis," Tribol. Int., vol. 114, pp. 349–357, 2017, doi: [10.1016/j.triboint.2017.04.041](https://doi.org/10.1016/j.triboint.2017.04.041).
- [15] S. Avikal, N. K. C. Kumar, A. R. Singh, et al., "Grey based Taguchi optimization for multi-lobe bearing," Mater. Today: Proc., vol. 26, no. 2, pp. 2663–2666, 2020, doi: [10.1016/j.matpr.2020.02.560](https://doi.org/10.1016/j.matpr.2020.02.560).
- [16] J. Sun, L. Shu, X. Song, et al., "Multi-objective optimization design of engine crankshaft bearing," Ind. Lubr. Tribol., vol. 68, no. 1, pp. 86–91, 2016, doi: [10.1108/ILT-03-2015-0040](https://doi.org/10.1108/ILT-03-2015-0040).
- [17] N. Biswas, P. Chakraborti, and P. Dhar, "Optimisation of Pressure and Oil Film Thickness in Multilobe Bearing using Response Surface Methodology and MOGA," J. Sci. Ind. Res., vol. 75, no. 8, pp. 495–499, 2016.
- [18] A. B. Shinde, P. M. Pawar, B. P. Ronge, P. K. Bhuse, A. K. Parkhe, and P. V. Jadhav, "Optimization of multiple performance characteristics of Surface Micro-Textured journal bearing," in Springer eBooks, 2019, pp. 377–389. doi: [10.1007/978-3-030-16962-6_39](https://doi.org/10.1007/978-3-030-16962-6_39).
- [19] S. K. Mandal, B. Bhattacharjee, N. Biswas, K. Choudhuri, and P. Chakraborti, "Application of nanofluids on various performance characteristics of hydrodynamic journal bearing—A review," Proc. IMechE, Part E: J. Process Mech. Eng., vol. 236, no. 3, pp. 1229–1238, 2021, doi: [10.1177/09544089211063995](https://doi.org/10.1177/09544089211063995).
- [20] N. Biswas, S. Biswas, B. Bhattacharjee, et al., "Prediction and Optimization of a Hydrodynamic Journal Bearing's Energy Efficient Tribological Behaviours for Different Grades of Lube Oil: A Novel DoE-RSM Strategy," Arab. J. Sci. Eng., vol. 49, pp. 11645–11660, 2024, doi: [10.1007/s13369-024-08829-6](https://doi.org/10.1007/s13369-024-08829-6).
- [21] S. K. Mandal, B. Bhattacharjee, N. Biswas, K. Choudhuri, and P. Chakraborti, "Parametric optimisation on the performance of the journal bearing using Taguchi approach," Proc. IMechE, Part E: J. Process Mech. Eng., 2023, doi: [10.1177/09544089231207477](https://doi.org/10.1177/09544089231207477).
- [22] N. Biswas, S. K. Mandal, I. Bhagwatkar, R. Kumar, J. Kaur, A. Bhowmik, K. Choudhuri, and B. Bhattacharjee, "Effect of nanoparticle-based lubricants on various performance characteristics of journal bearings: a review," Eng. Res. Express, vol. 7, no. 1, 012501, 2025, doi: [10.1088/2631-8695/ada8f7](https://doi.org/10.1088/2631-8695/ada8f7).
- [23] S. Baskar and G. Sriram, "Tribological behavior of journal bearing material under different lubricants," Tribol. Ind., vol. 36, no. 2, pp. 127–133, 2014.
- [24] Srinivas, M. Yunus, S. M. Munshi, and I. H. H., "Performance Evaluation of Hydrodynamic Journal Bearing using Gearbox and Engine Oil (SAE90 and SAE20w50) by Experimental and Theoretical Methods," Int. J. Mech. Eng. Inf. Tech., 2015, doi: [10.18535/ijmeit/v3i111.04](https://doi.org/10.18535/ijmeit/v3i111.04).
- [25] R. F. Lanes and R. D. Flack, "Effects of Three-Lobe bearing geometries on flexible rotor stability," A S L E Transactions, vol. 25, no. 3, pp. 377–385, 1982, doi: [10.1080/05698198208983105](https://doi.org/10.1080/05698198208983105).
- [26] N. Biswas, P. Chakraborti, A. Saha, and S. Biswas, "Performance & stability analysis of a three lobe journal bearing with varying parameters: Experiments and analysis," AIP Conference Proceedings, vol. 1754, p. 030002, 2016, doi: [10.1063/1.4958346](https://doi.org/10.1063/1.4958346).
- [27] R. D. Flack and P. E. Allaire, "An experimental and theoretical examination of the static characteristics of Three-Lobe bearings," A S L E Transactions, vol. 25, no. 1, pp. 88–94, 1982, doi: [10.1080/05698198208983069](https://doi.org/10.1080/05698198208983069).
- [28] D. F. Li, K. C. Choy, and P. E. Allaire, "Stability and transient characteristics of four multilobe journal bearing configurations," J. Lubr. Technol., vol. 102, no. 3, pp. 291–298, 1980, doi: [10.1115/1.3251514](https://doi.org/10.1115/1.3251514).
- [29] M. Aher, S. S. Belkar, and R. R. Kharde, "Pressure Distribution Analysis of Plain Journal Bearing with Lobe Journal Bearing," Int. J. Eng. Res. Technol., vol. 2, no. 1, pp. 1–6, 2013.
- [30] N. Biswas, P. Chakraborti, and S. Belkar, "An analytical and experimental approach for pressure distribution analysis of a particular lobe and plain bearing performance keeping in view of all impeding varying parameters associating with

- fixed lubrication SAE20W40," J. Mech. Sci. Technol., vol. 30, no. 5, pp. 2187–2193, 2016, doi: [10.1007/s12206-016-0426-9](https://doi.org/10.1007/s12206-016-0426-9).
- [31] A. D. Rahmatabadi, M. Nekoeimehr, and R. Rashidi, "Micropolar lubricant effects on the performance of noncircular lobed bearings," Tribol. Int., vol. 43, no. 1–2, pp. 404–413, 2009, doi: [10.1016/j.triboint.2009.07.002](https://doi.org/10.1016/j.triboint.2009.07.002).
- [32] S. C. Sharma, V. M. Phalle, and S. C. Jain, "Performance of a noncircular 2-lobe multirecess hydrostatic journal bearing with wear," Ind. Lubr. and Tribol., vol. 64, no. 3, pp. 171–181, 2012, doi: [10.1108/00368791211218704](https://doi.org/10.1108/00368791211218704).
- [33] A. Kumar, R. Sinhasan, and D. V. Singh, "Performance Characteristics of Two-Lobe Hydrodynamic Journal bearings," J. Lubr. Technol., vol. 102, no. 4, pp. 425–429, 1980, doi: [10.1115/1.3251576](https://doi.org/10.1115/1.3251576).
- [34] S. C. Soni, R. Sinhasan, and D. V. Singh, "Performance characteristics of noncircular bearings in laminar and turbulent flow regimes," A S L E Transactions, vol. 24, no. 1, pp. 29–41, 1981, doi: [10.1080/05698198108982995](https://doi.org/10.1080/05698198108982995).
- [35] A. Singh and B. K. Gupta, "Static and dynamic properties of oil films in displaced centres elliptical bearings," Proc. IMechE, Part C: J. Mech. Eng. Sci., vol. 197, no. 3, pp. 159–165, 1983, doi: [10.1243/pime_proc_1983_197_091_02](https://doi.org/10.1243/pime_proc_1983_197_091_02).
- [36] M. K. Ghosh and Satish, "Rotordynamic characteristics of multilobe hybrid bearings with short sills-part I," Tribol. Int., vol. 36, no. 8, pp. 625–632, 2003, doi: [10.1016/s0301-679x\(03\)00006-9](https://doi.org/10.1016/s0301-679x(03)00006-9).
- [37] A. Kumar and S. Kakoty, "Effect of couple stress parameter on steady-state and dynamic characteristics of three-lobe journal bearing operating on TiO₂ nanolubricant," Proc. IMechE, Part J: J. of Eng. Tribol., vol. 234, no. 4, pp. 528–540, 2019, doi: [10.1177/1350650119866028](https://doi.org/10.1177/1350650119866028).
- [38] A. R. Shooroki, A. D. Rahmatabadi, and M. Z. Mehrjardi, "Effect of using hybrid nano lubricant on the thermo-hydrodynamic performance of two lobe journal bearings," Proc. IMechE, Part J: J. of Eng. Tribol., vol. 236, no. 6, pp. 1167–1185, 2021, doi: [10.1177/13506501211053089](https://doi.org/10.1177/13506501211053089).
- [39] N. Tala-Ighil, M. Fillon, and P. Maspeyrot, "Effect of textured area on hydrodynamic journal bearing performance," Tribol. Int., vol. 44, no. 3, pp. 211–219, 2010, doi: [10.1016/j.triboint.2010.10.003](https://doi.org/10.1016/j.triboint.2010.10.003).
- [40] A. Kumar and S. K. Kakoty, "Variable viscosity analysis of three-lobe journal bearing with TiO₂ nanolubricant," Springer Manufacturing Engineering, 2019, doi: [10.1007/978-981-13-6287-3_1](https://doi.org/10.1007/978-981-13-6287-3_1).
- [41] A. A. Solghar, "Investigation of nanoparticle additive impacts on thermohydrodynamic characteristics of journal bearings," Proc. IMechE, Part J: J. of Eng. Tribol., vol. 229, no. 10, pp. 1176–1186, 2015, doi: [10.1177/1350650115574734](https://doi.org/10.1177/1350650115574734).
- [42] R. Nicoletti, "The importance of the heat capacity of lubricants with nanoparticles in the static behavior of journal bearings," J. Tribol., vol. 136, no. 4, 2014, doi: [10.1115/1.4027861](https://doi.org/10.1115/1.4027861).
- [43] S. B. Kalakada, P. N. Kumarapillai, and R. K. Perikinalil, "Analysis of static and dynamic performance characteristics of THD journal bearing operating under lubricants containing nanoparticles," Int. J. Precis. Eng. Manuf., vol. 13, no. 10, pp. 1869–1876, 2012, doi: [10.1007/s12541-012-0245-6](https://doi.org/10.1007/s12541-012-0245-6).
- [44] H. Sadabadi and A. S. Nezhad, "Nanofluids for Performance Improvement of Heavy Machinery Journal Bearings: A Simulation study," Nanomaterials, vol. 10, no. 11, p. 2120, 2020, doi: [10.3390/nano10112120](https://doi.org/10.3390/nano10112120).
- [45] A. Dhanola and H. C. Garg, "Experimental analysis of the efficacy of vegetable oil-based nanolubricants for improving journal-bearing performance," Proc. IMechE, Part J: J. of Eng. Tribol., vol. 235, no. 9, pp. 1974–1991, 2021, doi: [10.1177/1350650120981478](https://doi.org/10.1177/1350650120981478).
- [46] S. R. Suryawanshi and J. T. Pattiwar, "Experimental study on an influence of bearing geometry and TiO₂ nanoparticle additives on the performance characteristics of fluid film lubricated journal bearing," Tribol. Ind., vol. 41, no. 2, pp. 220–236, 2019, doi: [10.24874/ti.2019.41.02.08](https://doi.org/10.24874/ti.2019.41.02.08).
- [47] M. O. Yasir, S. Y. Ahmed, and B. A. Abass, "Performance analysis of experimentally characterized titanium dioxide and zinc oxide Nano-Lubricated Journal bearing considering thermal and cavitation effects," Arab. J. Sci. Eng., vol. 48, no. 3, pp. 3599–3614, 2022, doi: [10.1007/s13369-022-07219-0](https://doi.org/10.1007/s13369-022-07219-0).
- [48] T. P. Gundarneeeya and D. P. Vakharia, "Performance analysis of journal bearing operating on nanolubricants with TiO₂, CuO and Al₂O₃ nanoparticles as lubricant additives," Mater. Today, Proc., vol. 45, pp. 5624–5630, 2021, doi: [10.1016/j.matpr.2021.02.350](https://doi.org/10.1016/j.matpr.2021.02.350).
- [49] B. Bhattacharjee, P. Chakraborti, and K. Choudhuri, "Nano-fluid lubrication of single-layered porous hydrostatic bearing: a theoretical approach," J. Braz. Soc. Mech. Sci. & Eng., vol. 42, no. 7, 2020, doi: [10.1007/s40430-020-02446-8](https://doi.org/10.1007/s40430-020-02446-8).
- [50] D. Byotra, S. Sharma, A. Bangotra, and R. K. Awasthi, "Effect of nano-additives lubricant on the dynamic performance of textured journal

- bearing,” in CRC Press eBooks, 2023, pp. 215–235. doi: [10.1201/9781003306276-14](https://doi.org/10.1201/9781003306276-14).
- [51] S. K. Pradhan, R. Kumar, and P. C. Mishra, “Material modeling and optimization of rough elliptic bore journal bearing,” *Mater. Today, Proc.*, vol. 44, pp. 1021–1027, 2020, doi: [10.1016/j.matpr.2020.11.174](https://doi.org/10.1016/j.matpr.2020.11.174).
- [52] M. Rafiqhi, M. Özdemir, A. Şahinoğlu, R. Kumar, S. R. Das, “Experimental assessment and TOPSIS optimization of cutting force, surface roughness, and sound intensity in hard turning of AISI 52100 steel,” *Surf. Rev. Lett.*, vol. 29, no. 11, 2022, doi: [10.1142/S0218625X22501505](https://doi.org/10.1142/S0218625X22501505).
- [53] S. Mishra, S. Datta, and S. S. Mahapatra, “Grey-based and fuzzy TOPSIS decision-making approach for agility evaluation of mass customization systems,” *Benchmarking: An Int. J.*, vol. 20, no. 4, pp. 440–462, 2013, doi: [10.1108/bij-07-2011-0050](https://doi.org/10.1108/bij-07-2011-0050).
- [54] J. Zhao, Y. Huang, Y. He, and Y. Shi, “Nanolubricant additives: A review,” *Friction*, vol. 9, no. 5, pp. 891–917, 2020, doi: [10.1007/s40544-020-0450-8](https://doi.org/10.1007/s40544-020-0450-8).
- [55] C.-H. Lo, T.-T. Tsung, L.-C. Chen, C.-H. Su, and H.-M. Lin, “Fabrication of copper oxide nanofluid using submerged arc nanoparticle synthesis system (SANSS),” *J. Nanopart. Res.*, vol. 7, no. 2–3, pp. 313–320, 2005, doi: [10.1007/s11051-004-7770-x](https://doi.org/10.1007/s11051-004-7770-x).
- [56] J. A. Eastman et al., “Enhanced thermal conductivity through the development of nanofluids,” *MRS Online Proc. Library*, vol. 457, 1996, doi: [10.1557/proc-457-3](https://doi.org/10.1557/proc-457-3).
- [57] S. Lee, S. U. -s. Choi, S. Li, and J. A. Eastman, “Measuring thermal conductivity of fluids containing oxide nanoparticles,” *J. Heat Transfer*, vol. 121, no. 2, pp. 280–289, 1999, doi: [10.1115/1.2825978](https://doi.org/10.1115/1.2825978).
- [58] X. Wang, X. Xu, and S. U. S. Choi, “Thermal conductivity of nanoparticle - fluid mixture,” *J Thermophys Heat Trans.*, vol. 13, no. 4, pp. 474–480, 1999, doi: [10.2514/2.6486](https://doi.org/10.2514/2.6486).
- [59] S. M. S. Murshed, K. C. Leong, and C. Yang, “Enhanced thermal conductivity of TiO₂—water based nanofluids,” *Int. J. Therm. Sci.*, vol. 44, no. 4, pp. 367–373, 2005, doi: [10.1016/j.ijthermalsci.2004.12.005](https://doi.org/10.1016/j.ijthermalsci.2004.12.005).
- [60] K. Kwak and C. Kim, “Viscosity and thermal conductivity of copper oxide nanofluid dispersed in ethylene glycol,” *Korea-Aust. Rheol. J.*, vol. 17, no. 2, pp. 35–40, 2005.
- [61] B. Sharma, S. K. Sharma, S. M. Gupta, and A. Kumar, “Modified Two-Step method to prepare Long-Term Stable CNT nanofluids for heat transfer applications,” *Arab. J. Sci. Eng.*, vol. 43, no. 11, pp. 6155–6163, 2018, doi: [10.1007/s13369-018-3345-5](https://doi.org/10.1007/s13369-018-3345-5).
- [62] W. T. Urmi, A. S. Shafiqah, M. Rahman, K. Kadirgama, and A. Maleque, “Preparation Methods and Challenges of Hybrid Nanofluids: A Review,” *J. Adv. Res. Fluid Mech. Thermal Sci.*, vol. 78, no. 2, pp. 56–66, 2024.
- [63] G. Paul, J. Philip, B. Raj, P. K. Das, and I. Manna, “Synthesis, characterization, and thermal property measurement of nano-Al₉₅Zn₀₅ dispersed nanofluid prepared by a two-step process,” *Int. J. Heat Mass Transf.*, vol. 54, no. 15–16, pp. 3783–3788, 2011, doi: [10.1016/j.ijheatmasstransfer.2011.02.044](https://doi.org/10.1016/j.ijheatmasstransfer.2011.02.044).
- [64] R. Kumar, S. Roy, P. Gunjan, A. Sahoo, D. D. Sarkar, and R. K. Das, “Analysis of MRR and surface roughness in machining Ti-6Al-4V ELI Titanium alloy using EDM process,” *Procedia Manuf.*, vol. 20, pp. 358–364, 2018, doi: [10.1016/j.promfg.2018.02.052](https://doi.org/10.1016/j.promfg.2018.02.052).
- [65] R. Kumar, A. K. Sahoo, K. Satyanarayana, and G. V. Rao, “Some studies on cutting force and temperature in machining Ti-6Al-4V alloy using regression analysis and ANOVA,” *Int. J. Ind. Eng. Comput.*, vol. 4, no. 3, pp. 427–436, 2013, doi: [10.5267/j.ijiec.2013.03.002](https://doi.org/10.5267/j.ijiec.2013.03.002).
- [66] A. Edelbi, R. Kumar, A. K. Sahoo, and A. Pandey, “Comparative Machining Performance investigation of Dual-Nozzle MQL-Assisted ZNO and AL₂O₃ nanofluids in face milling of Ti-3Al-2.5V alloys,” *Arab. J. Sci. Eng.*, vol. 48, no. 3, pp. 2969–2993, 2022, doi: [10.1007/s13369-022-07072-1](https://doi.org/10.1007/s13369-022-07072-1).
- [67] R. S. Pawade and S. S. Joshi, “Multi-objective optimization of surface roughness and cutting forces in high-speed turning of Inconel 718 using Taguchi grey relational analysis (TGRA),” *Int. J. Adv. Manuf. Technol.*, vol. 56, no. 1–4, pp. 47–62, 2011, doi: [10.1007/s00170-011-3183-z](https://doi.org/10.1007/s00170-011-3183-z).
- [68] S. Chakraborty, P. Chatterjee, and P. P. Das, “A DoE-TOPSIS method-based meta-model for parametric optimization of non-traditional machining processes,” *J. Model. Manag.*, vol. 14, no. 2, pp. 430–455, 2019, doi: [10.1108/jm2-08-2018-0110](https://doi.org/10.1108/jm2-08-2018-0110).
- [69] C.-L. Hwang and K. Yoon, “Methods for multiple attribute decision making,” in *Lecture notes in economics and mathematical systems*, 1981, pp. 58–191. doi: [10.1007/978-3-642-48318-9_3](https://doi.org/10.1007/978-3-642-48318-9_3).
- [70] M. Yurdakul and Y. T. İç, “Development of a performance measurement model for manufacturing companies using the AHP and TOPSIS approaches,” *Int. J. Prod. Res.*, vol. 43, no. 21, pp. 4609–4641, 2005, doi: [10.1080/00207540500161746](https://doi.org/10.1080/00207540500161746).